Duration of Individual Relativistic Electron Microbursts: A Probe Into Their Scattering Mechanism

M. Shumko[1,2], L.W. Blum[3], and A.B. Crew[4]

[1]NASA's Goddard Space Flight Center, Greenbelt, Maryland, USA
[3]Universities Space Research Association, Columbia, Maryland, USA
[3]University of Colorado Boulder, Boulder, Colorado, USA
[2]Johns Hopkins University Applied Physics Laboratory, Laurel, Maryland, USA

Key Points:

- We identified relativistic microbursts observed by the SAMPEX satellite and quantified their duration
- The microburst duration interquartile range is 70-140 ms and shows trends in AE, L-shell, and MLT
- Which one do you like more. This version? In MLT, microburst durations are shortest at midnight and longest at noon—a similar trend to chorus element durations.
- Or this version? In MLT, microburst duration doubles between midnight and noon—a trend similar to chorus element durations.

Corresponding author: M. Shumko, `msshumko@gmail.com`

Abstract

We used the Solar Anomalous and Magnetospheric Particle Explorer (SAMPEX) to identify and quantify the duration of > 1 MeV electron microbursts. We investigated trends in the microburst duration as a function of geomagnetic activity, L-shell, and magnetic local time (MLT)—with the clearest trend in MLT. The shortest microbursts, with a median duration around 80 milliseconds, were observed near midnight MLT. Moreover, microburst duration increases from midnight and noon MLT—at noon, the median microburst duration doubles to 160 milliseconds. The increasing microburst duration as a function of MLT is similar to the whistler mode chorus rising tone element duration, but theory does not conclusively predict what chorus wave properties control microburst duration.

Plain Language Summary

Does this summary read well now?

Energetic electron microbursts are an intense form of naturally occurring particle precipitation from the outer Van Allen Radiation Belt into Earth's atmosphere. Microbursts are observed in, or just above, Earth's atmosphere, and are characterized by their short duration in time series data, often assumed to be less than a second. The impact of microburst precipitation on Earth's atmosphere is uncertain, but has been predicted to substantially degrade Mesospheric Ozone through the production of Odd Nitrogen and Odd Hydrogen molecules. Besides their environmental impact, we don't comprehensively understand how plasma waves, such as whistler mode chorus waves, scatter microbursts into our atmosphere. Therefore, in this study we quantified the duration of microbursts and used it as a proxy to study how microbursts are scattered by these waves. We found that microbursts and chorus waves share at least one strong statistical trend (correlation?): their duration roughly doubles between the anti-sunward and sunward regions of the outer radiation belt.

1 Introduction

Earth's outer Van Allen radiation belt electron population is in constant flux, governed by many processes that affect charged particles via, for example: radial transport, injections from the magnetotail, magnetopause shadowing, and local heating and loss into Earth's atmosphere due to wave-particle interactions (e.g. Ripoll et al., 2020, and references within). Whistler mode chorus (WMC) is just one type of plasma wave characterized by short (≈ 100 ms) rising tone elements, and perform a dual role in electron dynamics: accelerating electrons from 10s of keV to MeV energies, as well as pitch angle scattering electrons into the atmosphere (e.g. Li, Thorne, Angelopoulos, Bonnell, et al., 2009; Thorne, 2010; Horne & Thorne, 2003; Summers, 2005). One form of electron precipitation are microbursts: a transient and intense increase of electrons, with a subsecond duration. Microbursts were first observed by balloons in Earth's upper atmosphere, and later by satellites in low Earth orbit (LEO), and recently at high altitude near the magnetic equator (e.g. Anderson & Milton, 1964; Blake et al., 1996; Lorentzen et al., 2001; O'Brien et al., 2003; Douma et al., 2017; Kurita et al., 2016; Shumko et al., 2018).

Microburst electron energies span multiple orders of magnitude from tens of keV observed by, for example, Datta et al. (1997); to > 1 MeV observed by the Solar Anomalous Magnetospheric Particle Explorer (SAMPEX) by Blum et al. (2015). Microbursts are predominately observed outside the plasmapause on the radiation belt footprints, $L \approx 4 - 8$, and in the midnight to morning Magnetic Local Times (MLT) ($\approx 0 - 12$ hours MLT) (Lorentzen et al., 2001; Blum et al., 2015; O'Brien et al., 2003; Douma et al., 2017). While microbursts are observed under all geomagnetic conditions, Douma et al. (2017) showed that microburst frequency dramatically increases with the Auroral Electrojet (AE)

index, and O'Brien et al. (2003) showed a similar trend with the microburst frequency with the Disturbance storm time index.

The relative impact of microbursts on the ionization of Earth's atmosphere and the depletion of radiation belt electrons is uncertain cite Kathy's paper once it shows up online (Duderstadt et al., 2021), but the impact of microbursts alone is estimated to be substantial. Microbursts can deplete the outer radiation belt electrons in as little as a few hours, and can deplete up to 20% of upper mesospheric ozone (O'Brien et al., 2004; Thorne et al., 2005; Douma et al., 2019; Breneman et al., 2017; Seppälä et al., 2018).

Electron microbursts are widely believed to be scattered by chorus waves. They were associated early on, due to the similar duration of microbursts and chorus rising tone elements, and a similar occurrence distributions in MLT (e.g. Lorentzen et al., 2001). Breneman et al. (2017) directly linked a chorus rising tone element to a microburst observed by the Focused Investigation of Relativistic Electron Bursts: Intensity, Range, and Dynamics CubeSats (FIREBIRD-II; Crew et al. (2016); Johnson et al. (2020)) during a close magnetic conjunction. Drop this or add somewhere else: With this evidence, the particle precipitation community is largely in agreement that chorus waves scatter microbursts. Reword However, there are other hypothesized drivers such as electromagnetic ion cyclotron (Omura & Zhao, 2013; Douma et al., 2018).

A natural follow-on question is how are microbursts scattered. For example, it is still unclear if relativistic (>1 MeV) microbursts are scattered via cyclotron resonance at high magnetic latitudes, or a higher resonance harmonic near the magnetic equator (Lorentzen et al., 2001). One way to address this question is by studying for how long microburst electrons are in resonance with a chorus wave. The resulting microburst duration, i.e. the microburst width in the time series data, is a probe into the conditions necessary to scatter microburst electrons. From our review, we found only qualitative estimates of the microburst duration. Therefore, we used the microbursts observed by the SAMPEX satellite to quantify the distribution of relativistic microburst duration. In this letter, we quantify the duration distribution of microbursts as a function of L-shell, MLT, and the Auroral Electrojet. We then compare these results to prior chorus rising tone element studies, and a chorus-electron scattering model.

2 Instrumentation

In this study we used the >1 MeV electron count data, taken by the Heavy Ion Large Telescope (HILT) instrument (Klecker et al., 1993), onboard the SAMPEX satellite (Baker et al., 1993).

SAMPEX was launched in July 1992 and reentered Earth's atmosphere in November 2012. It was in a 520x670 km, 82° inclination low Earth orbit. In general, SAMPEX had two pointing modes: spin and orbit rate rotation (zenith pointing) modes. To avoid the compounding effects due to the variable pitch angles sampled in the spin mode, we only used the zenith pointing mode data. The International Geomagnetic Reference Field (Thébault et al., 2015, IGRF) magnetic field model was used to derive the meomagnetic coordinates.

We used the HILT electron data, sampled at a 20 ms cadence (state4 in the data archive), taken between 1997 and 2012. The HILT instrument consisted of a large rectangular chamber with the aperture on one end, and 16 solid state detectors on the other. The electron counts accumulated over 20 ms were summed from all of the solid state detectors and used in this study.

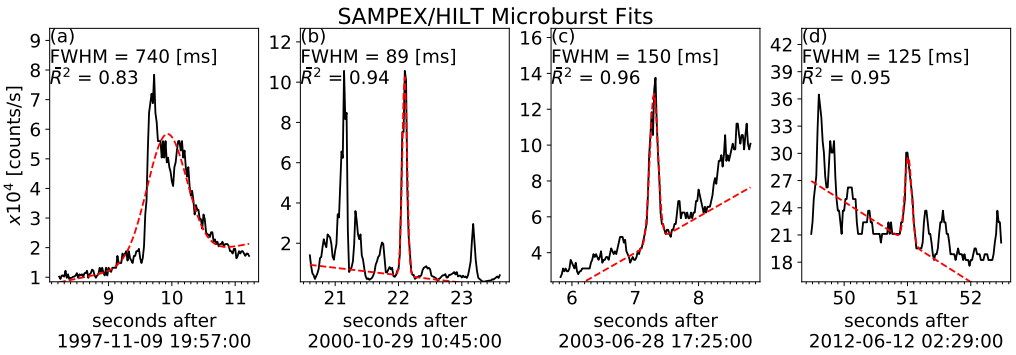

Figure 1. Examples of relativistic microbursts are shown by the black lines, and the fits are shown by the dashed red lines. The fit's full width at half maximum (FWHM) and the $\bar{R}^2$ goodness of fit metric is annotated in each panel. Microbursts with $\bar{R}^2 > 0.9$ were used for this study. The major time ticks are at every second, while the minor ticks are at every 100 milliseconds.

3 Methodology

We first identified microbursts. Then we fit every microburst's time series to a model, consisting of a Gaussian superposed with a straight line, to quantify the duration for each microburst.

3.1 Microburst Identification

We identified microbursts using the burst parameter defined by O'Brien et al. (2003) and used in numerous other microburst studies with SAMPEX (e.g. Douma et al., 2017). Assuming Poisson probability for the observed electron counts, the burst parameter is the number of standard deviations of a foreground signal above the background, expressed as

$$n_\sigma = \frac{N - A}{\sqrt{A + 1}} \tag{1}$$

where N is the number of foreground electron counts (microburst or otherwise), and A is the centered running average background counts. The 1 in the denominator prevents a division by 0 error. In O'Brien et al. (2003), and in the results in this study, N was summed over 100 ms and is called N_{100}, while A was summed over 500 ms and is similarly called A_{500}. Henceforth, we specify the time windows with subscripts for N and A. Times when $n_\sigma > 10$ are classified as burst times, and the time at the peak count rate in each continuos burst time interval is added to the microburst data set. With A_{500} and N_{100}, we detected a total of 256,764 microbursts over the 15 year period from 1997 to 2012. Four examples of microbursts are shown in Fig. 1 by the solid black curves.

3.2 Fitting to Quantify Microburst Duration

We estimated the microburst duration using two methods that yielded similar results: the duration at half of the microburst's topographic prominence and the full width at half maximum (FWHM) from a Gaussian fit.

The topographic prominence is a simple and robust method to estimate the microburst duration used to identify curtains, a similar-looking type of precipitation (Shumko et al., 2020). It is defined as the duration at half of the microburst's topographic prominence: the height of the microburst relative to the maximum of the two minima on either side of the microburst peak. On each side of the microburst peak, the minima are searched for between the microburst and a higher peak on that side. While the topographic

prominence method of estimating microburst durations is simple and robust, one of its downsides is its inability to automatically verify that the duration is representative of a single microburst. Therefore, we also fit microbursts with a Gaussian, and used the R^2 goodness of fit metric to filter out bad duration estimates. By screening out bad fits, we exclude superposition of multiple microbursts that will bias our microburst duration estimates.

We assumed a Gaussian superposed with a straight line fit model. The Gaussian models the shape of the microburst; while the linear trend accounts for the background electrons that are either trapped or quasi-trapped in the drift loss cone. The fit model is defined as:

$$c(t|A, t_0, \sigma, c_0, c_1) = Ae^{-\frac{(t-t_0)^2}{2\sigma^2}} + c_0 + c_1 t \tag{2}$$

where A, t_0, and σ are the Gaussian amplitude, center time, and standard deviation; while the c_0 and c_1 are the background count intercept and slope. The fit was applied over a number of data points determined by the maximum of either: 4x topographic prominence width or 500 ms. A challenge to any robust and automated nonlinear regression algorithm is guessing the initial parameters. The initial parameter guesses for the Gaussian are provided by the topographic prominence and topographic duration estimates. The two linear trend initial parameters were: $c_0 = \text{median(counts)}$ and $c_1 = 0$. The optimal fit parameters were found using scipy's `curve_fit()` function in Python. We defined the microburst duration as the FWHM of the microburst peak, defined by

$$\text{FWHM} = 2\sqrt{2\ln 2}\sigma. \tag{3}$$

To evaluate the fit, we used the R^2 goodness of fit metric. R^2 is defined as

$$R^2 = 1 - \frac{SS_{res}}{SS_{mean}} = 1 - \frac{\sum (c_i - f_i)^2}{\sum (c_i - \bar{c})^2} \tag{4}$$

where SS_{res} is the sum of the squared residuals between the observed counts c_i and the fit counts f_i for each time step, and likewise SS_{mean} is the sum of the squared residuals between c_i and the mean of the counts, $\bar{c}$.

One interpretation of R^2 is: fractionally how much better is the variance in the data explained by the model fit, compared to the null hypothesis horizontal line at $\bar{c}$. R^2 values vary from 1 when the fit perfectly describes the variance in the data, to $-\infty$ for poor fits (a fit can be much worse than the mean null hypothesis).

To account for overfitting that results from the variable number of data points used for each fit, the adjusted R^2, $\bar{R}^2$, was used. It is defined as

$$\bar{R}^2 = 1 - (1 - R^2)\frac{n-1}{n-p-1} \tag{5}$$

where n is the number of data points fit, and p is the number of parameters. Intuitively, $n-1$ is the number of degrees of freedom for the null hypothesis, and $n-p-1$ is the degrees of freedom for the fit model. Fits with $\bar{R}^2 > 0.9$ are considered good fits and are used for the rest of this analysis. As a check, we compared the microburst duration estimated with the prominence and fit methods. Does the following sentence make more sense now? We chose an agreement criterion between the two methods as durations within 25%; together with the $\bar{R}^2 > 0.9$ constraint, 85% of microbursts satisfied this agreement criterion.

Figure 1a shows an example of two superposed microbursts that had a fit $\bar{R}^2 = 0.83$ that were excluded from this study. On other hand, Fig. 1b-d show microbursts that were included in this study because the fit $\bar{R}^2 > 0.9$.

Lastly, Fig. 1c,d demonstrate the necessity of the linear fit to account for the changing background. The linear fit accounts for the non-zero mean background counts and

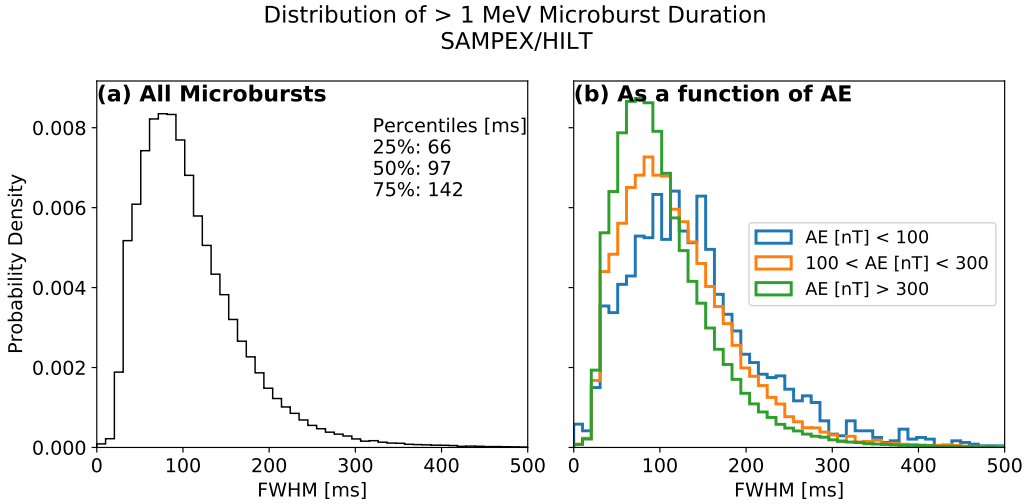

Figure 2. Panel a shows the distribution of all microburst full width at full maximum (FWHM). Panel b shows the distribution of all microbursts, categorized by the Auroral Electroject (AE) index into three bins: AE $<$ 100, 100 $<$ AE $<$ 300, and AE $>$ 300, in units of nanotesla. The median microburst duration is 130 ms for the AE $<$ 100 (2.4×10^3 microbursts), 111 ms for the 100 $<$ AE $<$ 300 (1.8×10^4 microbursts), and 95 ms for the AE $>$ 300 (9.3×10^4 microbursts) bins.

the different amplitudes of the edges of the Gaussian. Of the 256,764 detected microbursts, 109,231 had $\bar{R}^2 > 0.9$ and are used for the remainder of this study.

4 Results

We used the well-fit microbursts to quantify the distribution of microburst duration (FWHM) as a function of the Auroral Electrojet index, L-shell and MLT. We begin with the overall microburst distribution.

Figure 2a shows the distribution of all well-fit microbursts. This distribution is peaked with the median at 96 ms and quickly drops off. The interquartile range spans about a factor of two in microburst duration, from 65 to 139 ms. A new sanity check! As a check, we quantified the variation in the percentiles, annotated in Fig. 2a, under varying $\bar{R}^2$ criteria. We found that the percentile variation is minor—the median discrepancy between $\bar{R}^2 > 0.5$ and $\bar{R}^2 > 0.9$ thresholds is 4 ms.

We then investigated the dependence of microburst duration as a function of geomagnetic activity. To be consistent with the prior wave and microburst studies, we use the AE index to quantify the level of geomagnetic disturbance. We adopt the same three AE intensity levels used in prior studies, such as Li, Thorne, Angelopoulos, Bortnik, et al. (2009), Douma et al. (2017), and Meredith et al. (2020): AE $<$ 100, 100 $<$ AE $<$ 300, and AE $>$ 300, in units of nanotesla. Figure 2b shows the distribution of microburst duration for the three AE categories. The distributions are qualitatively similar, gradually narrowing and shifting to shorter durations with increasing AE. The median microburst duration decreases from 130 ms for AE $<$ 100 to 95 ms for AE $>$ 300.

Lastly, Figs. 3 and 4 show the microburst duration as a function of L and MLT. Figure 3a-c shows the joint distributions, split up into the 25th, 50th, and 75th percentiles; Figure 4 shows the marginalized distributions as a function of L or MLT.

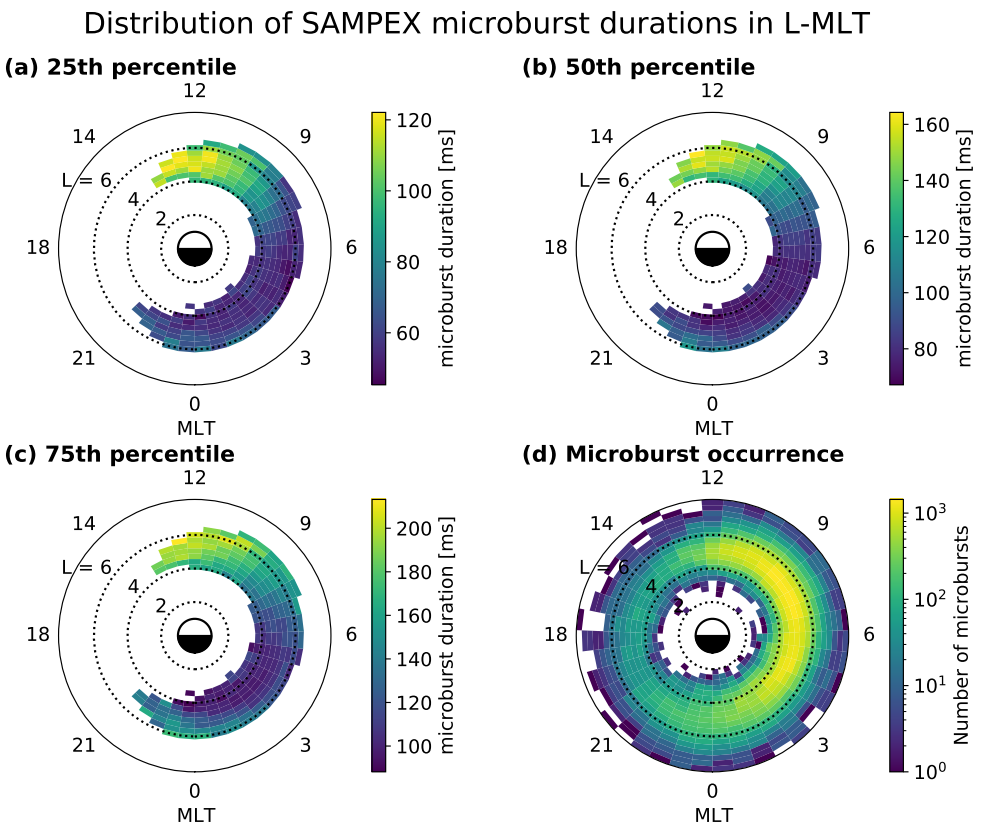

Figure 3. The joint distributions of microburst duration (FWHM) as a function of L-Shell and MLT. Panels a-c show the 25th, 50th, and 75th duration percentiles in each L-MLT bin. The white bins in panels a-c have a statistically insufficient number of microbursts (less than 100). Lastly, panel d shows the distribution of the number of microbursts, with the white bins containing 0 microbursts.

Figure 3 shows that the microburst duration trend is nearly identical for the different percentiles, and thus for simplicity we focus on the median distribution in Fig. 3b. In MLT, the median microburst duration increases by roughly a factor of two: from 80 ms at midnight to 160 ms at noon. In L-shell, the median microburst duration faintly increases with L-shell, and is most apparent near midnight MLT.

To disentangle the L and MLT distributions, Fig. 4 shows the marginalized distributions; MLT was marginalized out in Fig. 4a and L-shell was marginalized out in Fig. 4b. Figure 4a shows a slight broadening of the microburst duration at higher L-shells—in contrast to Fig. 4b that clearly shows that the microburst duration increases from midnight to noon MLT.

5 Discussion and Conclusions

We first discuss a possibility that the burst parameter is less sensitive to microbursts with longer durations and is therefore not detecting them. Recall from Section 3.1 that A is the running average counts, centered on the foreground counts N, and the burst parameter, $n_\sigma \sim N - A$. Now consider the following hypothesized scenario. Given a microburst with a 500 ms duration and the burst parameter centered on the peak, A_{500} com-

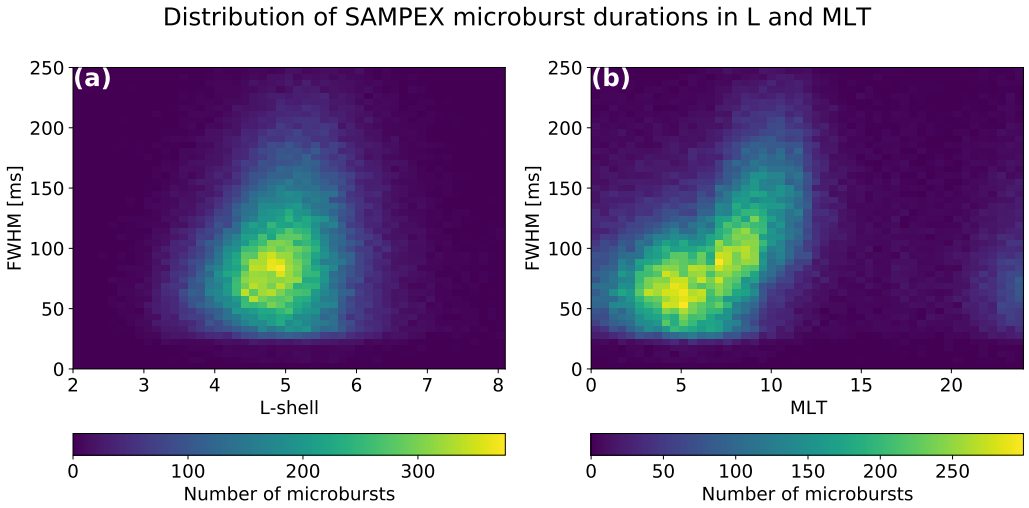

Figure 4. The marginalized distributions of the number of microbursts as a function of microburst duration (FWHM) and L shell in panel a and MLT in panel b.

pletely overlaps with the microburst and is therefore the mean microburst counts. Then, n_σ is proportional to the difference between the mean and the maximum microburst amplitude. However, if we use A_{1000}, the mean background counts no longer overlap with just the microburst, but rather the microburst and the lower surrounding background. The resulting A_{1000} is lower than A_{500} and thus the A_{1000} burst parameter is more sensitive to the microburst.

To test this possible bias, we ran the detection algorithm with three background values: A_{500}, A_{1000}, and A_{2000} and compared the resulting median distributions. The maximum discrepancy in the median microburst duration using the three resulting data sets was 20 ms (one data point); the longer median duration from a longer A. This is a 20% relative discrepancy. Consequently, considering this bias and the distribution in Fig. 2a, the evidence supports that the majority of > 1 MeV microbursts have a true duration around 100 ms and the A_{500} is adequate to identify them. With more confidence in the detection algorithm, we now shift to the global distribution of microburst durations.

The microburst duration trend in L-shell is subtle; Fig. 3c, and Fig. 4a most clearly show longer durations at higher L-shells near midnight MLT. In contrast, the duration trend in MLT is significant. The median microburst duration doubles from 80 to 160 ms between midnight and noon MLT. Now we will focus on the MLT trend and look for a possible explanation.

As mention in the introduction, chorus rising tone elements are widely believed to scatter microburst electrons (e.g. Breneman et al., 2017; Saito et al., 2012; Miyoshi et al., 2020). Thus, we will compare the microburst duration and chorus trends in local time. Recent studies by Teng et al. (2017) and Shue et al. (2019) quantified the properties of equatorial lower band (0.1-0.5 x electron gyrofrequency) chorus rising tone elements. Both studies found that the rising tone element duration distribution peaks at ≈ 250 ms around midnight, and this peak broadens and shifts to ≈ 500 ms at noon MLT. The microburst duration and chorus rising tone element trends in MLT scale by roughly the same factor of 2, but in general the chorus rising tone element duration is roughly 3 times longer

than > 1 MeV microbursts. However, theory points to a different chorus property controlling the microburst duration.

Figure 4 in Chen et al. (2020) shows the result of a microburst test particle simulation. The authors described what wave properties bound the microburst duration in time-energy space. Medium energy ($\approx 50-300$ keV) microburst duration is controlled by the rising tone element bandwidth. Moreover, higher energy microburst duration is controlled by the wave's lower frequency and the upper magnetic latitude propagation. This is in qualitative agreement with the cyclotron resonance condition described in Lorentzen et al. (2001), and the electron time of flight described by Saito et al. (2012).

While different model configurations may change what wave properties are theoretically responsible for scattering > 1 MeV microburst electrons, it is worth noting that Figs. 4 and 5 in Shue et al. (2019) do not show a clear shift in chorus bandwidth between midnight and noon MLT. Presently, the theory does not conclusively predict what chorus wave properties control the > 1 MeV microburst duration, but the chorus rising tone duration trend in MLT is worth further consideration.

As for the AE trend, the median microburst duration decreases from 130 ms, for $AE < 100$ nT, to 95 ms for $AE > 300$ nT. The chorus rising tone duration trend, quantified by Teng et al. (2017), is similar: it is broad and peaks at ≈ 500 ms when $AE < 100$ nT, then narrows and shifts to $\approx$ 250 ms when $AE >$ 300 nT. While both tend to become shorter with increased AE, the scaling factors are different.

Lastly, high latitude chorus waves, found at $\approx 10-25$ degrees magnetic latitude off of the equator, can also play at important role at scattering microburst electrons (Lorentzen et al., 2001). Li, Thorne, Angelopoulos, Bortnik, et al. (2009) found that the majority of high latitude chorus waves are constrained to 6-12 MLT. Thus, it is tempting to conclude that the microburst duration trend in MLT can be attributed to the low and high latitude chorus waves. However, because low latitude chorus waves are also observed at 0-12 MLT (Li, Thorne, Angelopoulos, Bortnik, et al., 2009), the resulting microburst duration distribution would reflect the chorus wave superposition in the 6-12 MLT region. If low and high latitude chorus waves scattered microbursts with different durations, Fig. 4b would show the durations broaden or bifurcate from midnight to noon MLT. Because Fig. 4b shows the microburst duration only shift to longer durations, high vs low latitude chorus waves are an unlikely explanation for the microburst duration trend in MLT.

In summary, we found that the relativistic microburst duration distribution is peaked at 100 ms, with 75% of microbursts narrower than 140 ms. We found no significant trend in the microburst duration as a function of L-shell, but we did find a strong trend as a function of MLT—the median microburst duration roughly doubles from 80 ms at midnight, to 160 ms at noon MLT. We found that the microburst duration trend in MLT scales similarly to the rising tone element duration, but the rising tone element duration is longer. Nonetheless, at this time theory is inconclusive: it does not predict that the relativistic microburst duration is controlled by the rising tone element duration, but rather by the chorus bandwidth and/or the upper latitude of propagation.

Acknowledgments

We are thankful for the engineers and scientists who made the SAMPEX mission possible. M. Shumko acknowledges the support provided by the NASA Postdoctoral Program at the NASA's Goddard Space Flight Center, administered by Universities Space Research Association under contract with NASA; L. Blum acknowledges the Heliophysics Innovation Fund program at NASA's Goddard Space Flight Center; and Alex's funding sources The SAMPEX HILT and attitude data are located at `http://www.srl.caltech.edu/sampex/DataCenter/data.html` and the minute cadence Auroral Electroject data is located at `ftp://ftp.ngdc.noaa.gov/STP/GEOMAGNETIC_DATA/INDICES/AURORAL_ELECTROJET/`

ONE_MINUTE/. This analysis software is available at: https://github.com/mshumko/sampex_microburst_widths, and is archived at Zenodo link (Clean up and document repo before v1.0 release is linked to Zenodo).

References

Anderson, K. A., & Milton, D. W. (1964). Balloon observations of X rays in the auroral zone: 3. High time resolution studies. *Journal of Geophysical Research*, *69*(21), 4457–4479. Retrieved from http://dx.doi.org/10.1029/JZ069i021p04457 doi: 10.1029/JZ069i021p04457

Baker, D. N., Mason, G. M., Figueroa, O., Colon, G., Watzin, J. G., & Aleman, R. M. (1993). An overview of the solar anomalous, and magnetospheric particle explorer (SAMPEX) mission. *IEEE Transactions on Geoscience and Remote Sensing*, *31*(3), 531–541.

Blake, J. B., Looper, M. D., Baker, D. N., Nakamura, R., Klecker, B., & Hovestadt, D. (1996). New high temporal and spatial resolution measurements by sampex of the precipitation of relativistic electrons. *Advances in Space Research*, *18*(8), 171 - 186. Retrieved from http://www.sciencedirect.com/science/article/pii/0273117795009698 doi: http://dx.doi.org/10.1016/0273-1177(95)00969-8

Blum, L., Li, X., & Denton, M. (2015). Rapid MeV electron precipitation as observed by SAMPEX/HILT during high-speed stream-driven storms. *Journal of Geophysical Research: Space Physics*, *120*(5), 3783–3794. Retrieved from http://dx.doi.org/10.1002/2014JA020633 (2014JA020633) doi: 10.1002/2014JA020633

Breneman, A., Crew, A., Sample, J., Klumpar, D., Johnson, A., Agapitov, O., ... others (2017). Observations directly linking relativistic electron microbursts to whistler mode chorus: Van allen probes and FIREBIRD II. *Geophysical Research Letters*.

Chen, L., Breneman, A. W., Xia, Z., & Zhang, X.-j. (2020). Modeling of bouncing electron microbursts induced by ducted chorus waves. *Geophysical Research Letters*, *47*(17), e2020GL089400. Retrieved from https://agupubs.onlinelibrary.wiley.com/doi/abs/10.1029/2020GL089400 (e2020GL089400 10.1029/2020GL089400) doi: https://doi.org/10.1029/2020GL089400

Crew, A. B., Spence, H. E., Blake, J. B., Klumpar, D. M., Larsen, B. A., O'Brien, T. P., ... Widholm, M. (2016). First multipoint in situ observations of electron microbursts: Initial results from the NSF FIREBIRD II mission. *Journal of Geophysical Research: Space Physics*, *121*(6), 5272–5283. Retrieved from http://dx.doi.org/10.1002/2016JA022485 (2016JA022485) doi: 10.1002/2016JA022485

Datta, S., Skoug, R., McCarthy, M., & Parks, G. (1997). Modeling of microburst electron precipitation using pitch angle diffusion theory. *Journal of Geophysical Research: Space Physics*, *102*(A8), 17325–17333.

Douma, E., Rodger, C., Blum, L., O'Brien, T., Clilverd, M., & Blake, J. (2019). Characteristics of relativistic microburst intensity from sampex observations. *Journal of Geophysical Research: Space Physics*.

Douma, E., Rodger, C. J., Blum, L. W., & Clilverd, M. A. (2017). Occurrence characteristics of relativistic electron microbursts from SAMPEX observations. *Journal of Geophysical Research: Space Physics*, *122*(8), 8096–8107. Retrieved from http://dx.doi.org/10.1002/2017JA024067 (2017JA024067) doi: 10.1002/2017JA024067

Douma, E., Rodger, C. J., Clilverd, M. A., Hendry, A. T., Engebretson, M. J., & Lessard, M. R. (2018). Comparison of relativistic microburst activity seen by sampex with ground-based wave measurements at halley, antarctica. *Journal*

of Geophysical Research: Space Physics, *123*(2), 1279–1294.

Duderstadt, K. A., Huang, C.-L., Spence, H. E., Smith, S., Blake, J. B., Crew, A. B., ... Vitt, F. M. (2021). Estimating the impacts of radiation belt electrons on atmospheric chemistry using firebird ii and van allen probes observations. *Journal of Geophysical Research: Atmospheres*, *n/a*(n/a), e2020JD033098. Retrieved from `https://agupubs.onlinelibrary.wiley.com/doi/abs/10.1029/2020JD033098` (e2020JD033098 2020JD033098) doi: https://doi.org/10.1029/2020JD033098

Horne, R. B., & Thorne, R. M. (2003). Relativistic electron acceleration and precipitation during resonant interactions with whistler-mode chorus. *Geophysical Research Letters*, *30*(10). Retrieved from `http://dx.doi.org/10.1029/2003GL016973` (1527) doi: 10.1029/2003GL016973

Johnson, A., Shumko, M., Griffith, B., Klumpar, D., Sample, J., Springer, L., ... others (2020). The FIREBIRD-II CubeSat mission: Focused investigations of relativistic electron burst intensity, range, and dynamics. *Review of Scientific Instruments*, *91*(3), 034503.

Klecker, B., Hovestadt, D., Scholer, M., Arbinger, H., Ertl, M., Kastele, H., ... others (1993). HILT: A heavy ion large area proportional counter telescope for solar and anomalous cosmic rays. *IEEE transactions on geoscience and remote sensing*, *31*(3), 542–548.

Kurita, S., Miyoshi, Y., Blake, J. B., Reeves, G. D., & Kletzing, C. A. (2016). Relativistic electron microbursts and variations in trapped mev electron fluxes during the 8–9 october 2012 storm: Sampex and van allen probes observations. *Geophysical Research Letters*, *43*(7), 3017-3025. Retrieved from `https://agupubs.onlinelibrary.wiley.com/doi/abs/10.1002/2016GL068260` doi: https://doi.org/10.1002/2016GL068260

Li, W., Thorne, R., Angelopoulos, V., Bonnell, J., McFadden, J., Carlson, C., ... Auster, H. (2009). Evaluation of whistler-mode chorus intensification on the nightside during an injection event observed on the THEMIS spacecraft. *Journal of Geophysical Research: Space Physics*, *114*(A1).

Li, W., Thorne, R. M., Angelopoulos, V., Bortnik, J., Cully, C. M., Ni, B., ... Magnes, W. (2009). Global distribution of whistler-mode chorus waves observed on the THEMIS spacecraft. *Geophysical Research Letters*, *36*(9). Retrieved from `http://dx.doi.org/10.1029/2009GL037595` (L09104) doi: 10.1029/2009GL037595

Lorentzen, K. R., Blake, J. B., Inan, U. S., & Bortnik, J. (2001). Observations of relativistic electron microbursts in association with VLF chorus. *Journal of Geophysical Research: Space Physics*, *106*(A4), 6017–6027. Retrieved from `http://dx.doi.org/10.1029/2000JA003018` doi: 10.1029/2000JA003018

Meredith, N. P., Horne, R. B., Shen, X.-C., Li, W., & Bortnik, J. (2020). Global model of whistler mode chorus in the near-equatorial region ($|\lambda_m| < 18°$). *Geophysical Research Letters*, *47*(11), e2020GL087311.

Miyoshi, Y., Saito, S., Kurita, S., Asamura, K., Hosokawa, K., Sakanoi, T., ... others (2020). Relativistic electron microbursts as high energy tail of pulsating aurora electrons.

O'Brien, T. P., Looper, M. D., & Blake, J. B. (2004). Quantification of relativistic electron microburst losses during the GEM storms. *Geophysical Research Letters*, *31*(4). Retrieved from `http://dx.doi.org/10.1029/2003GL018621` (L04802) doi: 10.1029/2003GL018621

O'Brien, T. P., Lorentzen, K. R., Mann, I. R., Meredith, N. P., Blake, J. B., Fennell, J. F., ... Anderson, R. R. (2003). Energization of relativistic electrons in the presence of ULF power and MeV microbursts: Evidence for dual ULF and VLF acceleration. *Journal of Geophysical Research: Space Physics*, *108*(A8). Retrieved from `http://dx.doi.org/10.1029/2002JA009784` doi: 10.1029/2002JA009784

Omura, Y., & Zhao, Q. (2013). Relativistic electron microbursts due to nonlinear pitch angle scattering by emic triggered emissions. *Journal of Geophysical Research: Space Physics*, *118*(8), 5008–5020.

Ripoll, J.-F., Claudepierre, S., Ukhorskiy, A., Colpitts, C., Li, X., Fennell, J., & Crabtree, C. (2020). Particle dynamics in the earth's radiation belts: Review of current research and open questions. *Journal of Geophysical Research: Space Physics*, *125*(5), e2019JA026735.

Saito, S., Miyoshi, Y., & Seki, K. (2012). Relativistic electron microbursts associated with whistler chorus rising tone elements: Gemsis-rbw simulations. *Journal of Geophysical Research: Space Physics*, *117*(A10), n/a–n/a. Retrieved from `http://dx.doi.org/10.1029/2012JA018020` (A10206) doi: 10.1029/2012JA018020

Seppälä, A., Douma, E., Rodger, C., Verronen, P., Clilverd, M. A., & Bortnik, J. (2018). Relativistic electron microburst events: Modeling the atmospheric impact. *Geophysical Research Letters*, *45*(2), 1141–1147.

Shue, J.-H., Nariyuki, Y., Katoh, Y., Saito, S., Kasahara, Y., Hsieh, Y.-K., ... Goto, Y. (2019). A systematic study in characteristics of lower band rising-tone chorus elements. *Journal of Geophysical Research: Space Physics*, *124*(11), 9003–9016.

Shumko, M., Johnson, A. T., O'Brien, T. P., Turner, D. L., Greeley, A. D., Sample, J. G., ... Halford, A. J. (2020). Statistical properties of electron curtain precipitation estimated with aerocube-6. *Journal of Geophysical Research: Space Physics*, *125*(12), e2020JA028462. Retrieved from `https://agupubs.onlinelibrary.wiley.com/doi/abs/10.1029/2020JA028462` (e2020JA028462 10.1029/2020JA028462) doi: https://doi.org/10.1029/2020JA028462

Shumko, M., Turner, D. L., O'Brien, T. P., Claudepierre, S. G., Sample, J., Hartley, D. P., ... Mitchell, D. G. (2018). Evidence of microbursts observed near the equatorial plane in the outer van allen radiation belt. *Geophysical Research Letters*, *45*(16), 8044-8053. Retrieved from `https://agupubs.onlinelibrary.wiley.com/doi/abs/10.1029/2018GL078451` doi: 10.1029/2018GL078451

Summers, D. (2005). Quasi-linear diffusion coefficients for field-aligned electromagnetic waves with applications to the magnetosphere. *Journal of Geophysical Research: Space Physics*, *110*(A8), n/a–n/a. Retrieved from `http://dx.doi.org/10.1029/2005JA011159` (A08213) doi: 10.1029/2005JA011159

Teng, S., Tao, X., Xie, Y., Zonca, F., Chen, L., Fang, W., & Wang, S. (2017). Analysis of the duration of rising tone chorus elements. *Geophysical Research Letters*, *44*(24), 12–074.

Thébault, E., Finlay, C. C., Beggan, C. D., Alken, P., Aubert, J., Barrois, O., ... others (2015). International geomagnetic reference field: the 12th generation. *Earth, Planets and Space*, *67*(1), 79.

Thorne, R. M. (2010). Radiation belt dynamics: The importance of wave-particle interactions. *Geophysical Research Letters*, *37*(22). Retrieved from `http://dx.doi.org/10.1029/2010GL044990` (L22107) doi: 10.1029/2010GL044990

Thorne, R. M., O'Brien, T. P., Shprits, Y. Y., Summers, D., & Horne, R. B. (2005). Timescale for MeV electron microburst loss during geomagnetic storms. *Journal of Geophysical Research: Space Physics*, *110*(A9). Retrieved from `http://dx.doi.org/10.1029/2004JA010882` (A09202) doi: 10.1029/2004JA010882